



# Pro-Arrhythmogenic Effects of Heterogeneous Tissue Curvature

## — A Suggestion for Role of Left Atrial Appendage in Atrial Fibrillation —

Jun-Seop Song; Jaehyeok Kim, BSc; Byounghyun Lim, PhD;  
Young-Seon Lee, PhD; Minki Hwang, PhD; Boyoung Joung, MD, PhD;  
Eun Bo Shim, PhD; Hui-Nam Pak, MD, PhD

**Background:** The arrhythmogenic role of complex atrial morphology has not yet been clearly elucidated. We hypothesized that bumpy tissue geometry can induce action potential duration (APD) dispersion and wavebreak in atrial fibrillation (AF).

**Methods and Results:** We simulated a 2D-bumpy atrial model by varying the degree of bumpiness, and 3D-left atrial (LA) models integrated by LA computed tomographic (CT) images taken from 14 patients with persistent AF. We also analyzed wave-dynamic parameters with bipolar electrograms during AF and compared them with LA-CT geometry in 30 patients with persistent AF. In the 2D-bumpy model, APD dispersion increased ( $P<0.001$ ) and wavebreak occurred spontaneously when the surface bumpiness was greater, showing phase transition-like behavior ( $P<0.001$ ). The bumpiness gradient 2D-model showed that spiral wave drifted in the direction of higher bumpiness, and phase singularity (PS) points were mostly located in areas with higher bumpiness. In the 3D-LA model, PS density was higher in the LA appendage (LAA) compared with other parts of the LA ( $P<0.05$ ). In 30 persistent-AF patients, the surface bumpiness of LAA was 5.8-fold that of other LA parts ( $P<0.001$ ), and exceeded critical bumpiness to induce wavebreak. Wave dynamics complexity parameters were consistently dominant in the LAA ( $P<0.001$ ).

**Conclusions:** Bumpy tissue geometry promoted APD dispersion, wavebreak, and spiral wave drift in in-silico human atrial tissue, and corresponded to clinical electroanatomical maps.

**Key Words:** Atrial fibrillation; Curvature; Left atrial appendage; Modeling

Atrial fibrillation (AF) is one of the most common cardiac arrhythmias that increases the risk of cardioembolic stroke and death. Although pulmonary vein isolation (PVI) is an effective treatment for AF, PVI-only ablation is not always sufficient, particularly in patients with persistent AF.<sup>1</sup> In 2010, Di Biase et al reported that the left atrial appendage (LAA) was responsible for atrial arrhythmias in 27% of patients undergoing redo ablation.<sup>2</sup> Several other clinical studies support that the LAA is a potential extrapulmonary source of atrial arrhythmias and that LAA isolation is effective for the treatment of persistent AF.<sup>3–6</sup> However, how the LAA plays a pro-arrhythmic role in the maintenance of AF has not been clearly revealed.

One of the significant features of the LAA is its complex bumpy morphology.<sup>7,8</sup> Several computational and experimental studies have shown that the uneven tissue geometry induces dispersion of the action potential duration (APD)<sup>9,10</sup> and changes spiral wave dynamics.<sup>8,11,12</sup> Rogers reported

that nonzero Gaussian curvature (briefly, ‘curvature’) of tissue geometry altered wave propagation speed and APD, and an abrupt change of curvature could promote wavebreak in ventricular geometry.<sup>13</sup> Despite being studied previously, the mechanism and arrhythmogenic role of bumpy atrial tissue have not been clearly established in human AF.

We hypothesized that bumpy tissue geometry could play a pro-arrhythmic role in AF. We studied the effects of heterogeneous curvature on spatial dispersion of the APD and wavebreak in in-silico human atrial tissue by varying the degree of bumpiness. To determine the pro-arrhythmic effects of bumpy feature in real LA geometry, we simulated a 3D-left atrial (LA) model reflecting the LA geometry of AF patients. Additionally, we measured surface bumpiness of the LAA, and estimated wave dynamics parameters from clinically obtained bipolar electrograms, such as complex fractionated atrial electrograms (CFAE), and entropy parameters (Shannon and approximate entropy), which

Received July 3, 2018; revised manuscript received September 2, 2018; accepted September 13, 2018; J-STAGE Advance Publication released online November 13, 2018 Time for primary review: 28 days

Yonsei University Health System, Seoul, Republic of Korea

Mailing address: Hui-Nam Pak, MD, PhD, Yonsei University Health System, 50 Yonsei-ro, Seodaemun-gu, Seoul 120-752, Republic of Korea. E-mail: hnpak@yuhs.ac

ISSN-1346-9843 All rights are reserved to the Japanese Circulation Society. For permissions, please e-mail: cj@j-circ.or.jp

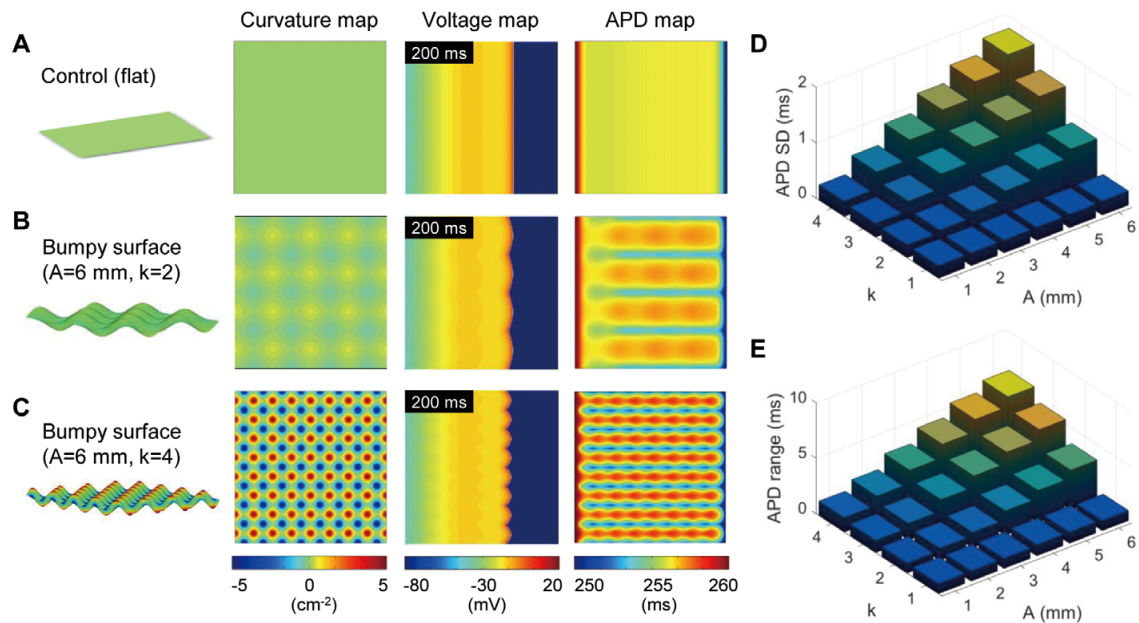


**Figure 1.** Spatial dispersion of the action potential duration (APD) in 2D-bumpy atrial tissue at 2 Hz line pacing from the left side. The APD was spatially heterogeneous in the bumpy surface and linearly correlated to curvature. (A–C) Curvature map, voltage map, and APD map are presented for the flat control case, bumpy surface of A=6 mm, k=2, and bumpy surface of A=6 mm, k=4, respectively. A and k are the amplitude and number of curves, respectively. (D,E) The degree of APD dispersion increased as surface bumpiness increased.

are known to be related to both wavebreak<sup>14</sup> and rotational activation.<sup>15,16</sup>

## Methods

### Computational Model of Bumpy Surface

We simulated homogeneous, isotropic bumpy tissue consisting of 512×512 human atrial cells ( $\Delta x=0.025$  cm). We designed periodically bumpy patterns by varying the degree of bumpiness as the following equation:

$$Z = A \sin\left(\frac{2\pi kx}{L}\right) \cos\left(\frac{2\pi ky}{L}\right)$$

where  $L=12.8$  cm is the size of the tissue,  $x$ ,  $y$  are coordinates of the cells ( $0 \leq x, y \leq L$ ),  $A$  (mm) is the amplitude of curves, and  $k$  (no unit) is the number of periodic curves. We constructed 24 surfaces by varying the amplitude of curves  $A=1\sim 6$  mm and the number of periodic curves  $k=1\sim 4$  (Supplementary Figure 1A). We considered flat tissue as the control case.

A biophysical model of the human atrial myocyte<sup>17</sup> was implemented. No electrical remodeling was assumed in order to determine the pure effect of bumpy geometry on wavebreak. We calculated electrical conduction by the following reaction-diffusion equation:

$$\frac{\partial V}{\partial t} = -\frac{I_{ion} + I_{stim}}{C_m} + D \nabla^2 V$$

where  $V$  (mV) is the transmembrane potential,  $C_m=100$  pF is the capacitance of the myocyte,  $I_{ion}$  and  $I_{stim}$  (pA) are the total transmembrane currents and stimulus current,

respectively, and  $D=0.001$  cm<sup>2</sup>/ms is the diffusion coefficient. The diffusion term  $\nabla^2 V$  was treated as the Laplace-Beltrami operator

$$\nabla^2 V = \frac{1}{\sqrt{g}} \sum_{i,j} \partial_i \left( \sqrt{g} g^{ij} \partial_j V \right)$$

where  $g^{ij}$  was the inverse of the metric  $g_{ij}$  and  $g$  was the determinant of the metric  $g_{ij}$  (Supplementary File).

To study the spatial dispersion of the APD in bumpy geometry, we measured the APD map at steady-state pacing. A vertical line located at the left side of the tissue was stimulated at 2 Hz, and the APD was measured across the grid at the 10th beat. The APD was calculated as the time interval between the time of maximum  $dV/dt$  and repolarization to  $-60$  mV, which is related to the effective refractory period.<sup>18</sup> The degree of APD dispersion was estimated by standard deviation (SD) and range (max-min) of the APD. We excluded the boundary region defined by 5% of the tissue size in the analysis to eliminate the effects of tissue boundary.

We initiated spiral wave using a S1S2 cross-field protocol. A vertical line was stimulated (S1), and further, horizontal half plane was stimulated (S2) when recovery front of S1 stimulus reached half of the tissue. After initiation of the spiral wave, we examined whether wavebreak spontaneously occurs for 5 seconds. Additionally, we reperformed all the simulations after standardizing the area of the surfaces.

In the above part, we designed the surfaces with uniformly bumpy patterns, however, real LA geometry containing both flat and complex bumpy structure has nonuniformly surface bumpiness. To examine how hetero-

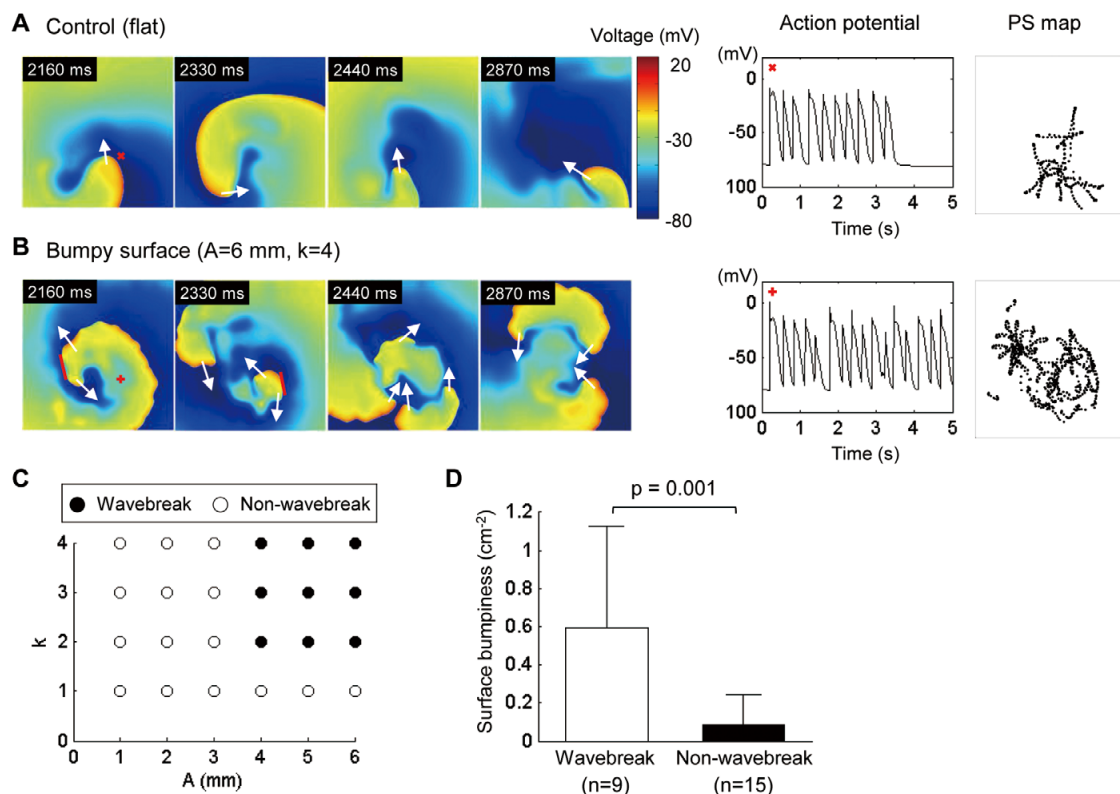


**Figure 2.** Formation of spontaneous wavebreak in a bumpy surface. In the 2D-bumpy model, bumpy geometry could induce wavebreak without the presence of electrical remodeling. (**A,B**) Snapshot of wave propagation, action potential, and phase singularity (PS) map are presented for flat control case and a bumpy surface of A=6 mm, k=4, respectively. A and k are the amplitude and number of curves, respectively. White arrows indicate direction of wave propagation and red lines indicate conduction block caused by refractoriness. Action potential recording points are marked by red symbols. (**C**) Spontaneous wavebreak occurred in highly bumpy surfaces (9 black dots). Surfaces with wavebreak are marked by black dots. White dots indicate that only a single spiral wave existed without any wavebreak. (**D**) Comparison of surface bumpiness between surfaces with wavebreak and other cases (Mann-Whitney U test,  $P=0.001$ ).

geneous bumpiness of atrial tissue affects spiral wave dynamics, we simulated 200 random Gaussian bumpy surfaces<sup>19</sup> and estimated wavebreak generation and AF sustainability defined as maintenance duration >5 s. Furthermore, we also applied the bumpiness gradient and/or the ionic current gradient to determine the effects of heterogeneous bumpiness on spiral wave drift. A detailed protocol is described in **Supplementary File**.

### Simulation of AF in 3D Human LA Model

We simulated an in-silico human LA model reflecting the LA anatomy of 14 AF patients (**Supplementary Table**) who underwent radiofrequency catheter ablation (RFCA), as previously described by Hwang et al.<sup>20</sup> The study protocol adhered to the Declaration of Helsinki and was approved by the Institutional Review Board of Yonsei University Health System. The written informed consent was obtained for the use of cardiac CT and RFCA data (clinicaltrials.gov; NCT02171364). The ionic current was calculated using a human atrial myocyte model<sup>17</sup> and electrical wave conduction was modeled by the mono-domain reaction-diffusion equation on the LA geometry (CUVIA, Model: SH01, ver. 1.0, Laonmed Inc.). We incorporated atlas-based

fiber orientation to represent anisotropic electrical conduction. After the induction of AF, we calculated the density of phase singular (PS) points<sup>21</sup> by dividing the number of PS points by the total number of nodes during 6 s of AF. A detailed protocol is described in **Supplementary File**.

### Clinical Electrophysiological Mapping of Wave Dynamics Parameters

We analyzed clinically obtained bipolar electrogram signals to evaluate the electrical wave dynamics of AF. Electrophysiological mapping was performed during sustained AF in 30 patients with persistent AF (22 men, 62.2±11.7 years old, **Supplementary Table**) who underwent RFCA (**Supplementary File**). The CFAE-cycle length (CL) was calculated by taking the average of the time intervals between consecutive deflections. The deflections were identified as downstroke morphology between the local-maximum and the local-minimum amplitudes within a time duration of 15 ms, which was set to avoid detection of far-field events. Additionally, we set a refractory period of 40 ms to avoid multiple detections of a single deflection event. CFAE was defined as CFAE-CL ≤120 ms.

We constructed a Shannon entropy (ShEn) map as

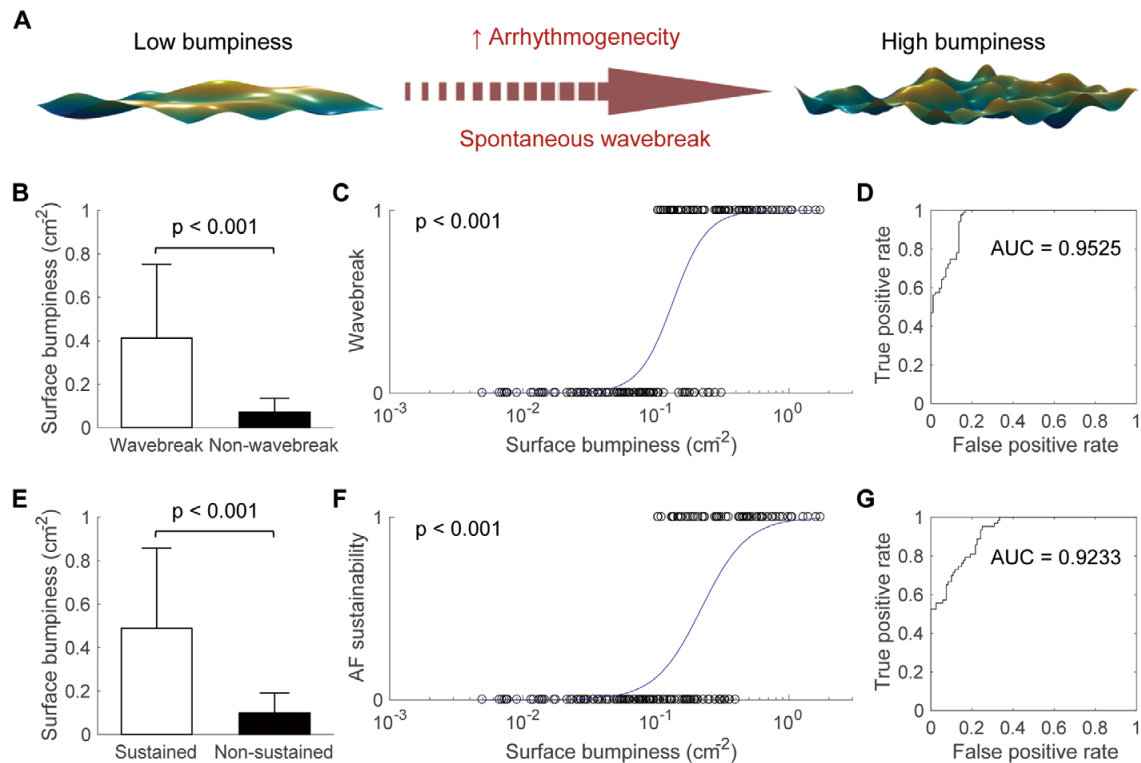


**Figure 3.** Phase transition-like behavior of spiral wave dynamics. **(A)** Random nonuniformly bumpy surfaces ( $n=200$ ) were generated for testing wavebreak generation and atrial fibrillation (AF) sustainability (duration  $>5$  s). **(B)** Comparison of bumpiness between wavebreak and non-wavebreak cases (t-test,  $P<0.001$ ). **(C)** Logistic regression analysis between wavebreak generation and bumpiness ( $P<0.001$ ). **(D)** Receiver-operating characteristic (ROC) analysis of the logistic regression model (area under the curve [AUC]=0.9525). **(E)** Comparison of bumpiness between AF-sustained and non-sustained cases (t-test,  $P<0.001$ ). **(F)** Logistic regression analysis between AF sustainability and bumpiness ( $P<0.001$ ). **(G)** ROC analysis of the logistic regression model (AUC=0.9233).

described by Ganesan et al.<sup>15</sup> Amplitude of the bipolar signal was binned into a voltage histogram (0.01 mV fixed bin size). The relative probability density  $P_i$  was calculated by dividing the number of counts in the  $i$ th bin by the sum of counts in all bins. The ShEn (no unit) was calculated as:

$$\text{ShEn} = - \sum_{i=0}^{N-1} P_i \log_2 P_i$$

where  $N$  is the total number of bins.

Additionally, we calculated an approximate entropy (ApEn) map to quantify the regularity of the bipolar signals.<sup>22</sup> We used standard parameters with embedding dimension  $m=2$  and threshold  $r=0.1$  as described by Orozco-Duque et al.<sup>16</sup>

### Calculation of Curvature and Surface Bumpiness

We calculated the curvature of tissue geometry at each node of the surface mesh.<sup>23</sup> To represent the degree of bumpiness of the surface, we defined “surface bumpiness” by the SD of the curvature as follows:

$$\text{Surface bumpiness} = \sqrt{\frac{1}{S} \iint (K - \bar{K})^2 dA}$$

where  $S$  ( $\text{cm}^2$ ) is the surface area,  $K$  ( $\text{cm}^{-2}$ ) is the curvature, and  $\bar{K}$  ( $\text{cm}^{-2}$ ) is the average of the curvature on the surface.

The surface bumpiness ( $\text{cm}^{-2}$ ) represents the heterogeneity of the curvature on the surface. The pulmonary veins and the mitral valve were excluded from the analysis.

### Statistical Analysis

All data are presented as mean  $\pm$  SD. Surface bumpiness and wave dynamics parameters were compared between the LAA and the other parts of the LA using a paired t-test. Linear correlation analysis was performed to determine the relationship between 2 continuous variables. All statistical analysis of small samples ( $n<30$ ) were performed with nonparametric tests. The relationship between the degree of APD dispersion and surface bumpiness was tested with Spearman correlation analysis. A  $P$ -value  $<0.05$  was considered to be statistically significant.

## Results

### Spiral Wave Dynamics in 2D-Bumpy Surface

**Dispersion of APD Depending on Curvature** In the 2D bumpy atrial model, we measured the APD map in steady-state pacing. There was heterogeneity of the APD induced by bumpy geometry in all 24 bumpy surfaces. As shown in the flat control case (**Figure 1A**), the APD was significantly changed in stimulation site and exit site despite zero-



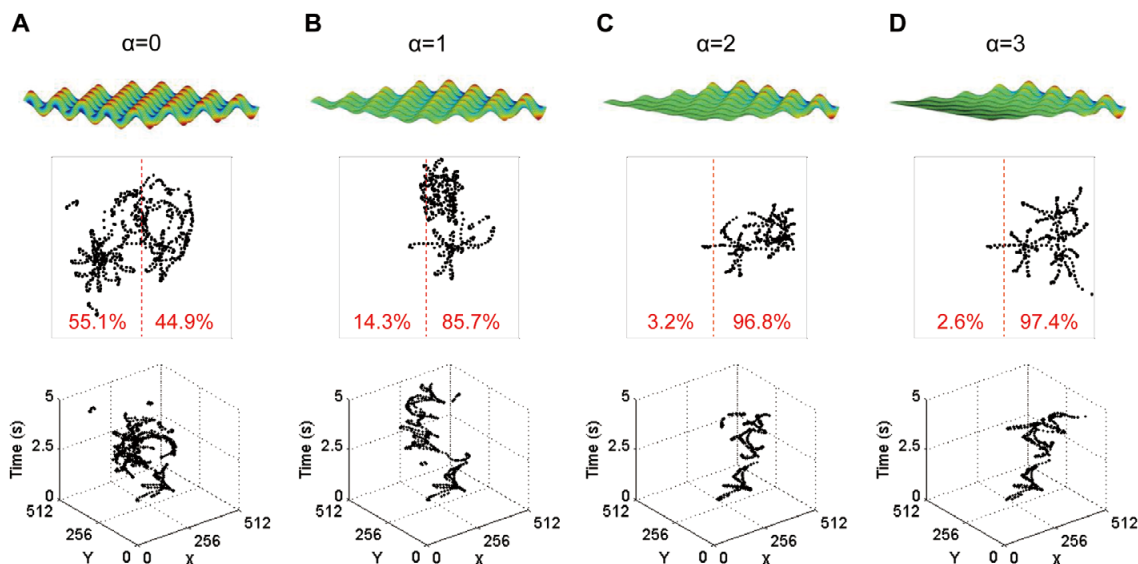


**Figure 4.** Spiral wave drift and wavebreak in a bumpy surface with a bumpiness gradient. In the 2D-bumpy model with a bumpiness gradient, the spiral wave drifted towards the highly bumpy region (right side). Phase singularity (PS) maps (middle row) and PS trajectories in space-time domain (bottom row) are presented for 4 different degrees of bumpiness gradient ( $\alpha=0, 1, 2, 3$ ). A portion of the PS points in the right half increased as the degree of bumpiness gradient increased (red numbers, %).

curvature of the tissue. This phenomenon is known as the “edge effect”.<sup>9</sup> To estimate the pure effect of curvature on APD dispersion, we excluded the boundary region in the analysis. In all 24 bumpy surfaces, there was a linear correlation between APD and curvature (the mean of 24 Pearson coefficients was  $R=0.4808 \pm 0.1931$ ,  $P<0.001$  for all 24 linear correlation tests). Additionally, the APD was more heterogeneous in highly bumpy surfaces. The degree of APD dispersion (SD and range of APD) increased with the higher amplitude and the greater number of curves (Figure 1D,E). Both the SD and range of APD had a positive correlation with the surface bumpiness (Spearman’s  $\rho=0.9809$  and  $0.9623$ , respectively, both  $P<0.001$ ).

**Formation of Wavebreak in Bumpy Geometry** We induced a single spiral wave and examined whether wavebreak occurred spontaneously. We considered the flat tissue as a control case to compare with bumpy tissue. In the flat control case (Figure 2A), only the single spiral wave existed without any formation of wavebreak until it spontaneously terminated. The PS map with the control case showed only a single trajectory of the spiral wave core. However, wavebreaks were observed in the 9 surfaces of high amplitude and number of curves (Figure 2C). As shown in Figure 2B, the wavefront was broken up into multiple wavelets when part of the wavefront failed to propagate in the region not yet recovered from refractoriness. The broken ends of the wavelets begin to rotate and these reentry centers were shown in the PS map. In the 9 surfaces with wavebreak, AF maintenance duration was prolonged compared with the flat control case ( $4.6 \pm 0.6$  vs.  $3.7$  s,  $P=0.004$ , Supplementary Figure 1B), and surface bumpiness was higher than in the other 15 surfaces ( $0.60 \pm 0.53$  vs.  $0.09 \pm 0.15 \text{ cm}^{-2}$ ,  $P=0.001$ , Figure 2D). We reperformed all the simulations after standardizing the area to eliminate the effects of tissue size on fibrillation. The results were consistent

with the original simulation (Supplementary Figure 1C,D).

Furthermore, we generated 200 random nonuniformly bumpy surfaces and determined whether wavebreak spontaneously generated and whether AF was maintained for 5 s in the fibrillating state (Figure 3). The surfaces with wavebreak had higher surface bumpiness than those in the non-wavebreak cases ( $P<0.001$ ), and the surface bumpiness of the AF-sustained cases was higher than that of the other cases ( $P<0.001$ ). The logistic regression model could predict wavebreak generation (odds ratio [OR]=934.68 [95% confidence interval (CI) 105.18–8306.01], area under the curve [AUC]=0.9525,  $P<0.001$ ) and AF sustainability (OR=45.45 [95% CI 12.28–168.19], AUC=0.9233,  $P<0.001$ ) from the surface bumpiness value.

**Drift of Spiral Wave Against Bumpiness Gradient** To determine the effects of heterogeneous bumpiness on spiral wave dynamics, we simulated a nonuniformly bumpy surface with a bumpiness gradient. In the uniformly bumpy case (Figure 4A), the spiral wave was sustained for  $>5$  s with wavebreaks, and more PS points were located in the left half of the plane than the right half of the plane (55.1% vs. 44.9%). However, in the surfaces with a bumpiness gradient (Figure 4B–D), more than 85% of the PS points were located in the right half plane, which had higher bumpiness than the left half plane (85.7%, 96.8%, 97.4% for  $\alpha=1, 2, 3$ , respectively). The spiral wave drifted towards the area of higher surface bumpiness.

The combined gradient of bumpiness and ionic current showed that PS points were concentrated in the area with higher levels of bumpiness and wavebreak occurred spontaneously; however, the spiral wave drift was not prominent and might have been masked by the electrical gradient (Supplementary Figure 2).

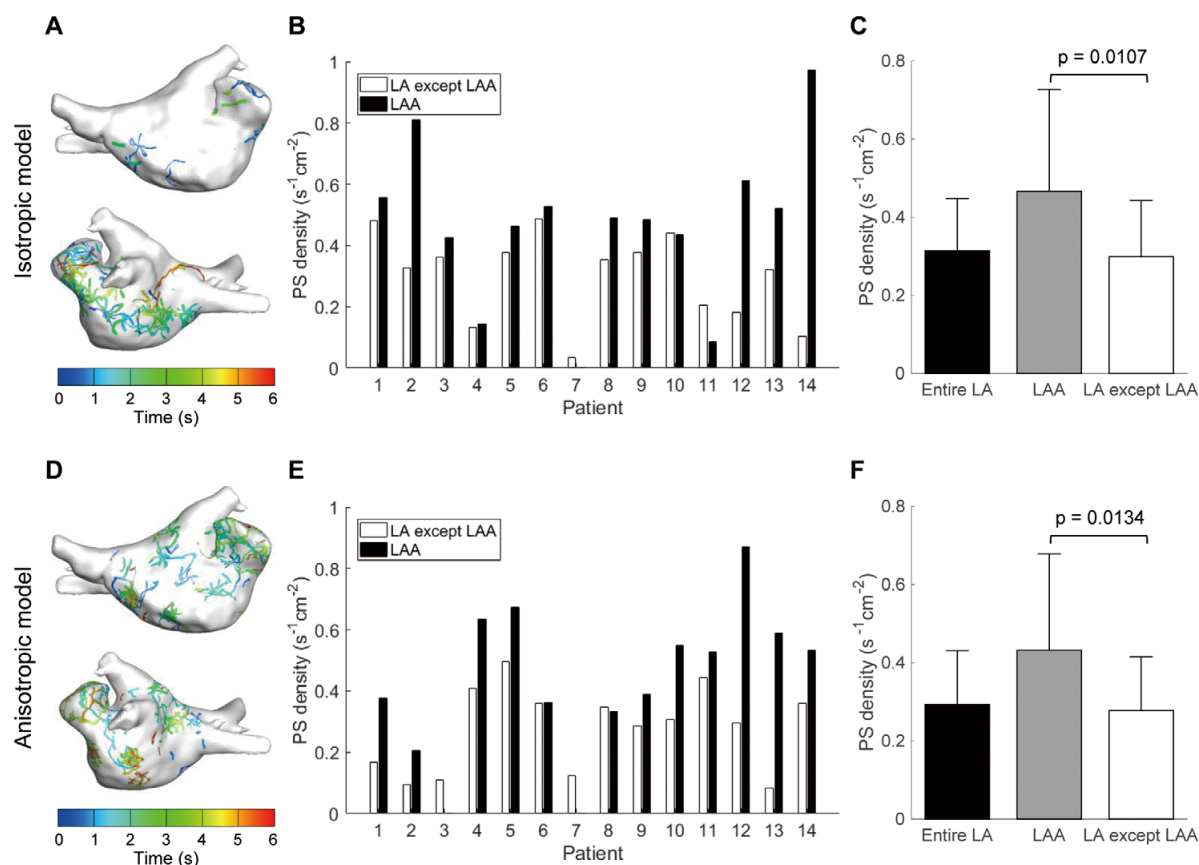


**Figure 5.** Phase singularity (PS) map in 3D left atrial (LA) model (n=14). In in-silico 3D LA model of atrial fibrillation (AF), AF was successfully induced and wavebreak occurred. **(A)** Representative PS map in the isotropic model. **(B,C)** comparison of PS density between LAA and other parts of the LA in the isotropic model (Wilcoxon signed-rank test,  $P=0.0107$ ). **(D)** Example of PS map in the anisotropic model. **(E,F)** Comparison of PS density in the LAA and other parts of the LA in the anisotropic model reflecting fiber orientation (Wilcoxon signed-rank test,  $P=0.0134$ ).

### 3D Human AF Simulation

To determine the formation of spontaneous wavebreak in the LAA, we simulated a 3D human AF model reflecting the LA anatomy of 14 AF patients. In all cases, AF was maintained for >6s and wavebreak was observed in the entire LA including the LAA. Because PS is known to be closely related to wavebreak,<sup>24</sup> we generated the PS map for 6s in the AF state. In both the isotropic and anisotropic models, the PS density in the LAA was significantly greater than in the other parts of the LA (**Figure 5**).

### Clinical Evidence for Arrhythmogenic LAA

**Curvature Map of LA Geometry** In 30 patients with persistent AF, we measured the curvature of the LA geometry reconstructed from CT images. **Figure 6A** shows that the curvature of LA geometry was heterogeneous over the entire LA. The surface bumpiness in the LAA was 5.8-fold compared with the other parts of the LA ( $1.52 \pm 0.33$  vs.  $0.26 \pm 0.04 \text{ cm}^{-2}$ ,  $P < 0.001$ , **Figure 6E**). All bumpiness values of the LAA had more than 99% probability of wavebreak generation according to the logistic regression model developed from the 2D simulation (**Figure 3**).

**Wave Dynamics Parameters of Bipolar Electrogram** We clinically obtained CFAE-CL, ShEn, and ApEn maps of

the same group of 30 patients with contact bipolar electrograms taken during clinical procedures (**Figure 6B–D**). Both parameters were utilized for evaluating the complexity of the fractionated electrogram, which is known to be closely related to wavebreak.<sup>14</sup> The CFAE-CL in the LAA was lower than that for the other parts of the LA ( $130.9 \pm 29.4$  vs.  $154.7 \pm 32.2 \text{ ms}$ ,  $P < 0.001$ ), and the percentage area of CFAE was higher in the LAA than in the other parts of the LA ( $40.1 \pm 22.0$  vs.  $30.1 \pm 14.5\%$ ,  $P < 0.001$ , **Figure 6F**). Moreover, there was an inverse relationship between the surface bumpiness of the LAA and the mean CFAE-CL of the entire LA ( $R = -0.376$ ,  $P = 0.041$ ). Additionally, both ShEn and ApEn in the LAA were higher compared with the rest of the LA (ShEn:  $4.40 \pm 0.66$  vs.  $3.50 \pm 0.39$ ; ApEn:  $0.10 \pm 0.04$  vs.  $0.04 \pm 0.02$ ; both  $P < 0.001$ , **Figure 6G**).

### Discussion

We have discovered the arrhythmogenic role of bumpy tissue geometry using a computational model of human atrial tissue. In the 2D-bumpy surface model, bumpy geometry induced APD dispersion, which led to formation of wavebreak at high levels of surface bumpiness. Addi-

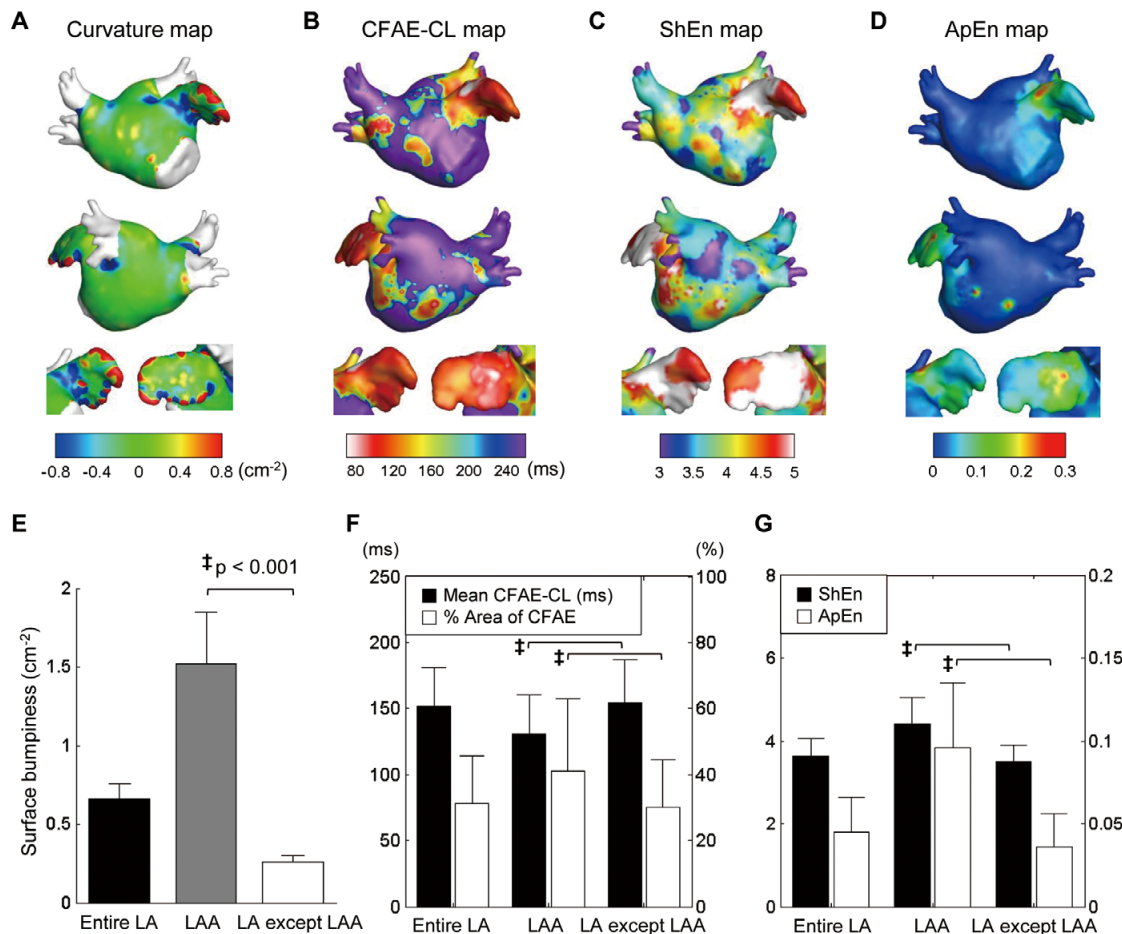


**Figure 6.** The 3D left atrial (LA) mapping of curvature, complex fractionated atrial electrogram-cycle length (CFAE-CL), Shannon entropy (ShEn), and approximate entropy (ApEn) for patients with persistent atrial fibrillation (n=30). Wave dynamics parameters were calculated from clinically recorded bipolar electrograms. All parameters were dominant in the LA appendage (LAA). (**A–D**) Examples of curvature, CFAE-CL, ShEn, and ApEn map, respectively. Anterior and posterior parts of the LA and LAA are displayed. (**E**) Surface bumpiness in the LAA and other parts of the LA (paired t-test,  $P < 0.001$ ). (**F**) Mean CFAE-CL and percentage area of CFAE (CFAE-CL  $\leq 120$  ms) in the LAA and other parts of the LA. (**G**) Entropy parameters (ApEn and ShEn) in the LAA and other parts of the LA (paired t-test,  $^{\dagger}P < 0.001$ ).

tionally, heterogeneous bumpiness caused spiral wave drift towards the region with higher surface bumpiness.

In the 3D-LA geometry, LAA showed significantly high levels of surface bumpiness, which produced spontaneous wavebreak in the 2D-bumpy model. We performed a 3D AF simulation and analyzed clinically obtained wave dynamics parameters. Both the simulation and clinical data showed that the parameters of wave dynamics were significantly higher in the LAA compared with other parts of the LA.

#### Effects of Bumpy Geometry on Spiral Wave Dynamics

The role of the curvature of tissue geometry in electrical wave dynamics was primarily discovered by Davydov and Zykov.<sup>11</sup> They theoretically explained the drift of spiral waves on a nonuniformly curved surface. Several computational and experimental studies showed that tissue shape, structural heterogeneity, boundary features, and activation time could induce heterogeneity of refractoriness,<sup>9,10</sup> which has been known to play an important role in the initiation

of reentry<sup>25</sup> and generation of wavebreaks.<sup>13,26</sup> We have discovered a quantitative relationship between APD heterogeneity and the curvature of tissue geometry, and its role in wavebreak generation in bumpy surfaces. Additionally, we found that the bumpy tissue geometry can localize PS points by attracting the spiral wave against the bumpiness gradient. This novel finding supports that not only ionic current heterogeneity,<sup>27,28</sup> but also structural heterogeneity contributes to spiral wave drift.<sup>29</sup> Therefore, higher surface bumpiness of tissue geometry may be a potential source of arrhythmia.

The effect of the curvature of tissue geometry can be mathematically explained by the diffusion equation of electrical conduction.<sup>30</sup> Under the assumption of isotropic conduction, the diffusion term can be represented by inverse metric of the surface as  $D \sum g^{ij} \partial_i \partial_j V$  where  $D$  is the diffusion coefficient and  $g^{ij}$  is the inverse metric of the surface. If we define “adjusted diffusion coefficient” as  $\tilde{D}_{ij} = D \cdot g^{ij}$ , the diffusion term can be expressed as  $\sum \tilde{D}_{ij} \partial_i \partial_j V$ . Therefore, heterogeneous curvature is mathe-

matically equivalent to heterogeneous and anisotropic conduction, which are already known to be important arrhythmogenic factors in cardiac fibrillation.<sup>26</sup>

### Roles of the LAA in AF Maintenance

According to the study of Di Biase et al,<sup>2</sup> 27% of patients undergoing redo ablation have the LAA as the trigger site of AF. Recently, they reported results of a 24-month follow-up in the BELIEF trial showing that LAA isolation improved the success rate of AF treatment in patients with long-standing persistent AF.<sup>4</sup> There are several potential mechanisms to describe the arrhythmogenic role of the LAA.<sup>7</sup> Because the embryological origin of the LAA is mesodermal myocardium, which is related to the opening of the pulmonary vein, the LAA may act similar to the PVs in the initiation of AF. Another anatomic consideration is the ligament of Marshall located between the LAA and the left superior PV. It contains sympathetic and parasympathetic nerves, which can form a triggering source of AF. Additionally, the complex fiber orientation of the LAA may influence wave propagation and formation of localized reentry in the LAA.<sup>3</sup>

We propose another potential mechanism of the bumpy morphology of the LAA contributing to the arrhythmogenesis of AF. As shown in **Figure 3**, we observed critical phase transition-like phenomenon, which implied that an extremely bumpy structure such as the LAA has the potential to generate wavebreak and to maintain AF. The simulation result and the clinical data indicated the presence of wavebreak or spiral wave reentry in the LAA. According to previous studies, CFAE, ShEn, and ApEn indicate the complexity of the fractionated electrogram, which is closely related to wavebreak and the arrhythmogenic characteristics of AF.<sup>14–16</sup> Additionally, high entropy parameters are known to be associated with rotational activation called “rotor”,<sup>15,16</sup> which is usually produced by wavebreak at the broken ends of wavelets.<sup>24</sup> Therefore, overall the results of our study implied that the bumpy morphology of the LAA may play a pro-arrhythmic role in human AF.

### Clinical Implications

Although much clinical evidence has emerged to support the efficacy of LAA isolation in controlling AF,<sup>2–6</sup> the mechanism of the LAA in the maintenance of AF is still unrevealed. We proposed a potential mechanism by which the bumpy morphology of the LAA may play a pro-arrhythmic role in AF. Of course, tissue heterogeneity and autonomic neural activity significantly contribute to the initiation and maintenance of arrhythmia. However, we found that anatomic bumpiness of cardiac structures also contributes to APD dispersion and arrhythmogenesis. Additionally, local bumpiness linearly correlates with LA wall thickness, which is closely associated with local wave dynamics parameters.<sup>31</sup> Therefore, not only evaluation of tissue heterogeneity but also measurement of surface bumpiness may contribute to accurate mapping of the potential target of arrhythmia in ablation procedures.

### Study Limitations

In the 2D simulation, we only considered a periodic bumpy pattern without testing the global structural heterogeneity of the LAA, which must play a role in atrial arrhythmogenicity. Also, we simulated 12.8×12.8 cm<sup>2</sup> tissue to avoid the issue of critical mass hypothesis.<sup>32,33</sup> However, quantitative results from a 2D simulation cannot be directly compared

with either simulation results of a 3D-LA model or real-world electrical wave dynamics in patients with AF, because of topological discrepancies such as the existence of tissue boundaries. In our 3D AF model, we did not consider regional LA wall thickness, tissue heterogeneity, or autonomic neural activity in order to test the exclusive role of bumpy tissue morphology and to reduce the computational cost, despite the increasing role of intramural conduction in AF.<sup>34</sup> The sample size of the 3D-patient-specific modeling was relatively small, which could have affected the results. However, we confirmed reproducible results in both parametric and nonparametric analyses. Because of technical limitations in accessing clinical APD and PS data from patients with AF, we considered CFAE-CL and ShEn as parameters for estimating electrical wave dynamics; however, CFAE-CL also reflects sequentially acquired electrograms with low spatial resolution, far-field potential, overlapped myocardial fibers, and AF drivers.<sup>14</sup> Complex nonlinear relationships between structural heterogeneity and wave dynamics should be further investigated.

### Conclusions

In a computational model of human atrial tissue, bumpy tissue morphology induced APD dispersion, which promoted formation of spontaneous wavebreak. Additionally, a bumpiness gradient caused spiral wave drift in the direction of areas of higher bumpiness. In the 3D-LA geometry, surface bumpiness of the LAA was significantly higher than in the other parts of the LA. Both simulation results and clinical data showed that wave dynamics parameters were significantly higher in the LAA than in the rest of the LA, implying a potential arrhythmogenic role of the LAA in human AF.

### Acknowledgments

This work was supported by a grant [A085136] from the Korea Health 21 R&D Project, Ministry of Health and Welfare and a grant [NRF-2017R1A2B4003983] from the Basic Science Research Program run by the National Research Foundation of Korea (NRF) which is funded by the Ministry of Science, ICT & Future Planning.

### Name of Grant

A grant [HI18C0070] from the Korea Health 21 R&D Project, Ministry of Health and Welfare. A grant [NRF-2017R1A2B4003983] from the Basic Science Research Program run by the National Research Foundation of Korea (NRF).

### References

1. Elayi CS, Verma A, Di Biase L, Ching CK, Patel D, Barrett C, et al. Ablation for longstanding permanent atrial fibrillation: Results from a randomized study comparing three different strategies. *Heart Rhythm* 2008; **5**: 1658–1664.
2. Di Biase L, Burkhardt JD, Mohanty P, Sanchez J, Mohanty S, Horton R, et al. Left atrial appendage: An underrecognized trigger site of atrial fibrillation. *Circulation* 2010; **122**: 109–118.
3. Hocini M, Shah AJ, Nault I, Sanders P, Wright M, Narayan SM, et al. Localized reentry within the left atrial appendage: Arrhythmogenic role in patients undergoing ablation of persistent atrial fibrillation. *Heart Rhythm* 2011; **8**: 1853–1861.
4. Di Biase L, Burkhardt JD, Mohanty P, Mohanty S, Sanchez JE, Trivedi C, et al. Left atrial appendage isolation in patients with longstanding persistent AF undergoing catheter ablation: BELIEF Trial. *J Am Coll Cardiol* 2016; **68**: 1929–1940.
5. Reissmann B, Rillig A, Wissner E, Tilz R, Schluter M, Sohns C, et al. Durability of wide-area left atrial appendage isolation: Results from extensive catheter ablation for treatment of persistent atrial fibrillation. *Heart Rhythm* 2017; **14**: 314–319.



6. Yorgun H, Canpolat U, Kocyigit D, Coteli C, Evranos B, Aytemir K. Left atrial appendage isolation in addition to pulmonary vein isolation in persistent atrial fibrillation: One-year clinical outcome after cryoballoon-based ablation. *Europace* 2017; **19**: 758–768.
7. Naksuk N, Padmanabhan D, Yogeswaran V, Asirvatham SJ. Left atrial appendage: Embryology, anatomy, physiology, arrhythmia and therapeutic intervention. *JACC Clin Electrophysiol* 2016; **2**: 403–412.
8. Yamazaki M, Mironov S, Taravant C, Brec J, Vaquero LM, Bandaru K, et al. Heterogeneous atrial wall thickness and stretch promote scroll waves anchoring during atrial fibrillation. *Cardiovasc Res* 2012; **94**: 48–57.
9. van Oosterom A, Jacquemet V. The effect of tissue geometry on the activation recovery interval of atrial myocytes. *Physica D Nonlinear Phenomena* 2009; **238**: 962–968.
10. Walton RD, Benson AP, Hardy ME, White E, Bernus O. Electrophysiological and structural determinants of electrotonic modulation of repolarization by the activation sequence. *Front Physiol* 2013; **4**: 281.
11. Davydov VA, Zykov VS. Kinematics of spiral waves on nonuniformly curved surfaces. *Physica D Nonlinear Phenomena* 1991; **49**: 71–74.
12. Khariche SR, Biktasheva IV, Seemann G, Zhang H, Biktashev VN. A computer simulation study of anatomy induced drift of spiral waves in the human atrium. *BioMed Research Int* 2015; **2015**: 731386.
13. Rogers JM. Wave front fragmentation due to ventricular geometry in a model of the rabbit heart. *Chaos* 2002; **12**: 779–787.
14. Atienza F, Calvo D, Almendral J, Zlochiver S, Grzeda KR, Martinez-Alzamora N, et al. Mechanisms of fractionated electrograms formation in the posterior left atrium during paroxysmal atrial fibrillation in humans. *J Am Coll Cardiol* 2011; **57**: 1081–1092.
15. Ganesan AN, Kuklik P, Lau DH, Brooks AG, Baumert M, Lim WW, et al. Bipolar electrogram shannon entropy at sites of rotational activation: Implications for ablation of atrial fibrillation. *Circ Arrhythm Electrophysiol* 2013; **6**: 48–57.
16. Orozco-Duque A, Ugarte JP, Tobón C, Saiz J, Bustamante J. Approximate entropy can localize rotors, but not ectopic foci during chronic atrial fibrillation: A simulation study. *Computing in Cardiology Conference* 2013; **40**: 903–906.
17. Courtemanche M, Ramirez RJ, Nattel S. Ionic mechanisms underlying human atrial action potential properties: Insights from a mathematical model. *Am J Physiol* 1998; **275**: H301–H321.
18. Kneller J, Zou R, Vigmond EJ, Wang Z, Leon LJ, Nattel S. Cholinergic atrial fibrillation in a computer model of a two-dimensional sheet of canine atrial cells with realistic ionic properties. *Circ Res* 2002; **90**: E73–E87.
19. Garcia N, Stoll E. Monte Carlo calculation for electromagnetic-wave scattering from random rough surfaces. *Phys Rev Lett* 1984; **52**: 1798–1801.
20. Hwang M, Kwon SS, Wi J, Park M, Lee HS, Park JS, et al. Virtual ablation for atrial fibrillation in personalized in-silico three-dimensional left atrial modeling: Comparison with clinical catheter ablation. *Prog Biophys Mol Biol* 2014; **116**: 40–47.
21. Lee YS, Song JS, Hwang M, Lim B, Joung B, Pak HN. A new efficient method for detecting phase singularity in cardiac fibrillation. *PLoS One* 2016; **11**: e0167567.
22. Pincus SM. Approximate entropy as a measure of system complexity. *Proc Natl Acad Sci USA* 1991; **88**: 2297–2301.
23. Stokely EM, Wu SY. Surface parametrization and curvature measurement of arbitrary 3-D objects: Five practical methods. *IEEE Trans Pattern Anal* 1992; **14**: 833–840.
24. Chen J, Mandapati R, Berenfeld O, Skanes AC, Gray RA, Jalife J. Dynamics of wavelets and their role in atrial fibrillation in the isolated sheep heart. *Cardiovasc Res* 2000; **48**: 220–232.
25. Clayton RH, Holden AV. Dispersion of cardiac action potential duration and the initiation of re-entry: A computational study. *Biomed Eng Online* 2005; **4**: 11.
26. Xie F, Qu Z, Garfinkel A, Weiss JN. Electrophysiological heterogeneity and stability of reentry in simulated cardiac tissue. *Am J Physiol Heart Circ Physiol* 2001; **280**: H535–H545.
27. Calvo CJ, Deo M, Zlochiver S, Millet J, Berenfeld O. Attraction of rotors to the pulmonary veins in paroxysmal atrial fibrillation: A modeling study. *Biophys J* 2014; **106**: 1811–1821.
28. Ten Tusscher KH, Panfilov AV. Reentry in heterogeneous cardiac tissue described by the Luo-Rudy ventricular action potential model. *Am J Physiol Heart Circ Physiol* 2003; **284**: H542–H548.
29. Dierckx H, Brisard E, Verschelde H, Panfilov AV. Drift laws for spiral waves on curved anisotropic surfaces. *Phys Rev E Stat Nonlin Soft Matter Phys* 2013; **88**: 012908.
30. Ogawa N. Curvature-dependent diffusion flow on a surface with thickness. *Phys Rev E Stat Nonlin Soft Matter Phys* 2010; **81**: 061113.
31. Song JS, Wi J, Lee HJ, Hwang M, Lim B, Kim TH, et al. Role of atrial wall thickness in wave-dynamics of atrial fibrillation. *PLoS One* 2017; **12**: e0182174.
32. Hwang M, Park J, Lee YS, Park JH, Choi SH, Shim EB, et al. Fibrillation number based on wavelength and critical mass in patients who underwent radiofrequency catheter ablation for atrial fibrillation. *IEEE Trans Biomed Eng* 2015; **62**: 673–679.
33. Qu Z. Critical mass hypothesis revisited: Role of dynamical wave stability in spontaneous termination of cardiac fibrillation. *Am J Physiol Heart Circ Physiol* 2006; **290**: H255–H263.
34. Hansen BJ, Zhao J, Csepe TA, Moore BT, Li N, Jayne LA, et al. Atrial fibrillation driven by micro-anatomic intramural re-entry revealed by simultaneous sub-epicardial and sub-endocardial optical mapping in explanted human hearts. *Eur Heart J* 2015; **36**: 2390–2401.

### Supplementary Files

Please find supplementary file(s);  
<http://dx.doi.org/10.1253/circj.CJ-18-0615>